Journal of Surface Engineered Materials and Advanced Technology, 2026, 16(1), 1-9
https://www.scirp.org/journal/jsemat
ISSN Online: 2161-489X
ISSN Print: 2161-4881

Numerical Analysis of Donor-Induced Band Gap Narrowing in InGaN Alloys for Photovoltaic Applications

Sada Traore[1,2*], Philippe Bernard Himbane[2], Moustapha Thiame[3]

[1]Laboratory of Semiconductor and Solar Energy, Cheikh Anta Diop University, Dakar, Senegal
[2]Laboratory of Electronics, Computer Science, Telecommunications and Renewable Energies, Gaston Berger University, Saint-Louis, Senegal
[3]Laboratory of Chemical and Physics of Materials, Assane Seck University, Ziguinchor, Senegal
Email: *sadatraore59@yahoo.fr

How to cite this paper: Traore, S., Himbane, P.B. and Thiame, M. (2026) Numerical Analysis of Donor-Induced Band Gap Narrowing in InGaN Alloys for Photovoltaic Applications. *Journal of Surface Engineered Materials and Advanced Technology*, **16**, 1-9.
https://doi.org/10.4236/jsemat.2026.161001

Received: November 15, 2025
Accepted: January 27, 2026
Published: January 30, 2026

Copyright © 2026 by author(s) and Scientific Research Publishing Inc.
This work is licensed under the Creative Commons Attribution International License (CC BY 4.0).
http://creativecommons.org/licenses/by/4.0/

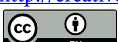
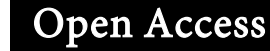

Abstract

This paper presents a systematic numerical analysis of the Band Gap Narrowing (BGN) effect in indium gallium nitride (InGaN) solar cells for two indium molar fractions ($x = 0.12$ and $x = 0.28$) at $T = 300$ K. By sweeping the donor doping concentration N from 10^{16} to 3×10^{18} cm^{-3}, we quantify the reduction of the effective band gap energy (E_{geff}) and the resulting red-shift of the optical cutoff wavelength (λ_{cut}). Results show that BGN intensifies non-linearly with doping and is systematically more pronounced for higher indium content. At the highest doping level (3×10^{18} cm^{-3}), λ_{cut} shifts by +154 nm for $x = 0.12$ and by +378 nm for $x = 0.28$, extending absorption deep into the visible spectrum. These findings underline the necessity of a careful trade-off between spectral coverage and material quality degradation in the design of high-efficiency InGaN photovoltaic devices.

Keywords

InGaN, Solar Cells, Band Gap Narrowing, Indium Molar Fraction, Cutoff Wavelength, III-Nitride Semiconductors

1. Introduction

The InGaN alloy (indium-gallium nitride) occupies a strategic position in the field of materials for photovoltaic conversion. Its tunable bandgap spans the spectrum from 0.7 eV (pure InN) to 3.51 eV (pure GaN) through simple variation of the indium molar fraction x. This makes it an ideal material for the fabrication of

multi-junction solar cells capable of covering the entire solar spectrum [1]-[4].

However, InGaN-based solar cells face significant physical constraints during fabrication. Doping, which is necessary to form p-n junctions, introduces high charge carrier concentrations that alter the intrinsic electronic properties of the material. One of the most significant effects is Band Gap Narrowing (BGN), a phenomenon in which the effective bandgap narrows due to Coulomb interactions between free carriers and between carriers and ionized impurities [5].

A quantitative understanding of BGN is essential for accurately predicting the spectral response of the solar cell and optimizing its conversion efficiency. Recent numerical studies on InGaN solar cells confirm that doping, active layer thickness, and device architecture simultaneously influence optical absorption, open-circuit voltage, and overall efficiency [6]-[9].

The present study proposes a comparative and systematic analysis of the effect of doping on BGN, the effective bandgap energy $\boldsymbol{E_{geff}}$, and the cutoff wavelength $\boldsymbol{\lambda_{cut}}$, for two representative InGaN compositions ($x = 0.12$ and $x = 0.28$) at a temperature of 300 K.

2. Theoretical Model

2.1. Bandgap Energy of InGaN

The bandgap energy of the $In_xGa_{1-x}N$ alloy as a function of the indium molar fraction x is given by the modified Vegard's law including the Varshni correction [10]:

$$E_g^{InGaN}(x,T) = x \cdot E_g^{InN}(T) + (1-x) \cdot E_g^{GaN}(T) - 1.43x \cdot (1-x) \quad (1)$$

where $\boldsymbol{b = 1.43}$ **eV** is the bowing parameter [1]. The Varshni parameters from Vurgaftman & Meyer (2003) are given in **Table 1**.

Temperature Dependence: Varshni's Law

For the binary compounds, the following expression is generally used:

$$\begin{cases} E_g^{InN}(T) = E_g^{InN}(0) - \dfrac{\alpha_{InN} T^2}{T + \beta_{InN}} \\ E_g^{GaN}(T) = E_g^{GaN}(0) - \dfrac{\alpha_{GaN} T^2}{T + \beta_{GaN}} \end{cases}$$

where α and β are material-specific constants. For the alloy, the temperature dependence follows the modified Vegard's law. E_g^{InN} and E_g^{GaN} are the bandgap energies of InN and GaN, respectively, and b is the bowing parameter.

Table 1. Varshni parameters and material properties [10]-[12].

Parameter	Symbol	GaN	InN	Unit	Reference
Bandgap at 0 K	$E_g(0)$	3.510	0.675	eV	Vurgaftman (2003)
Varshni α	α	9.09×10^{-4}	2.45×10^{-4}	eV/K	Vurgaftman (2003)
Varshni β	β	830	624	K	Vurgaftman (2003)
Electron effective mass	m_n^*	$0.20\ m_0$	$0.11\ m_0$	—	Vurgaftman (2003)

Continued

Hole effective mass	m_p^*	0.80 m_0	0.60 m_0	—	Vurgaftman (2003)
Static permittivity	ε_r	8.9	15.3	—	Levinshtein (2001)
Bowing parameter	b	1.43		eV	Wu *et al.* (2002)

2.2. Band Gap Narrowing (BGN) - Jain-Roulston Model

Band Gap Narrowing results from many-body interactions in heavily doped semiconductors: carrier-carrier exchange interactions, correlation effects, and ion-carrier interactions. For an n-type semiconductor, the bandgap reduction ΔE_{BGN} is modeled according to the Jain-Roulston formalism [5]:

$$E_{BGN}^{JR}(x,N,T) = A(x,N)\cdot N^{\frac{1}{3}} + B(x,N)\cdot N^{\frac{1}{4}} + C(x,N)\cdot \frac{1}{\lambda_D(x,N,T)} \quad (2)$$

where A, B, and C are material constants that depend on the composition x, and N is the doping concentration in cm^{-3}. where N denotes the donor concentration (N_D). Throughout this work, complete donor ionization at $T = 300$ K is assumed, so that the free electron concentration is approximated by $n \approx N_D$.

These coefficients are determined from the Jain-Roulston relation:

$$A(x,N) = \frac{1.83}{r_s^*(x,N)\cdot 4\pi\varepsilon_s(x)}\cdot\frac{\Lambda}{N_b^{\frac{1}{3}}} \quad (3)$$

$$B(x,N) = \frac{0.95}{r_s^{*3/4}(x,N)}\cdot\frac{q^2}{4\pi\varepsilon_s(x)} \quad (4)$$

$$C(x,N) = \frac{1.57}{r_s^{*3/2}(x,N)}\cdot\frac{q^2}{4\pi\varepsilon_s(x)}\cdot\frac{m_d^*(x)}{m^*(x)} \quad (5)$$

where the reduced Wigner-Seitz radius is given by:

$$r_s^*(x,N) = \left(\frac{3}{4\pi N}\right)^{1/3}\cdot\frac{m^*(x)}{m_0}\cdot\frac{1}{a_B^*(x)} \quad (6)$$

$$a_B^*(x) = \frac{4\pi\varepsilon_s(x)\hbar^2}{m^*(x)q^2} \quad (7)$$

where λ_D is the Debye length given by the following equation:

$$\lambda_D(x,N) = \sqrt{\frac{\varepsilon_s(x)k_BT}{q^2N}} \quad (8)$$

The material parameters (m_n^*, m_p^*, ε_r) are linearly interpolated between the values of GaN and InN as a function of x.

$$m^*(x) = xm_{InN}^* + (1-x)m_{GaN}^*,\quad m^*(x) = xm_{InN}^* + (1-x)m_{GaN}^* \quad \text{et}$$
$$\varepsilon_s(x) = x\varepsilon_{InN} + (1-x)x\varepsilon_{GaN}$$

These parameters are given in **Table 2**.

Table 2. Some values of the electrical properties of GaN and InN at 300 K.

Property	InN	GaN
Band gap (E_g) eV	0.675	3.51
Electron affinity (χ) eV	5.6	4.1
Effective density of states in the conduction band (N_c) (cm^{-3})	$5.1 \cdot 10^{17}$	$2.3 \cdot 10^{18}$
Effective density of states in the valence band (N_v) (cm^{-3})	$5.3 \cdot 10^{19}$	$4.6 \cdot 10^{19}$
Electron effective mass (m_e)	$0.11m_0$	$0.2m_0$
Hole effective mass (m_h)	0.65	$0.80\ m_0$
Dielectric permittivity (ε)	15.3	8.9

2.3. Validity Range of the Jain-Roulston Model

The Jain-Roulston model is valid for doping concentrations $N \le 3 \times 10^{18}\ \mathrm{cm}^{-3}$. Beyond this limit, two physical effects not included in the model become significant: Although the Jain–Roulston model was originally developed for conventional semiconductors such as Si, Ge and GaAs, it has been widely employed as a first-order approximation for evaluating many-body interaction effects in heavily doped III-V semiconductors. The predicted BGN magnitudes obtained in this study remain within the order of magnitude reported for heavily doped GaN and InGaN materials in the literature, supporting the applicability of the model for comparative analysis.

Burstein-Moss effect: Band filling by degenerate carriers leads to an apparent increase in the optical bandgap, which partially compensates the Band Gap Narrowing (BGN).

Carrier degeneracy: The Fermi level penetrates into the conduction band, invalidating the classical Boltzmann statistics used in the derivation of the Jain-Roulston model.

2.4. Effective Bandgap and Cutoff Wavelength

The cutoff wavelength λ_{cut} corresponds to the minimum photon energy required to excite an electron across the effective bandgap. The relations for the effective bandgap energy and the cutoff wavelength are given by the following equation:

$$E_g^{InGaN}(x,N,T) = E_g(x,T) - E_{BGN}^{JR}(x,N,T) \quad \lambda_{cut}(\mathrm{nm}) = \frac{1240}{E_{geff}[\mathrm{eV}]} \tag{9}$$

A red shift of λ_{cut} (*i.e.*, an increase) indicates the possibility of absorbing photons of lower energy. This can increase the short-circuit current density Jsc but may potentially degrade the open-circuit voltage Voc, as shown by several recent numerical optimization studies on single-junction InGaN structures, thin polar layers, and intermediate-band architectures [6]-[8] [13].

3. Results and Discussion

3.1. Summary of Parameters as a Function of Doping

Table 3 and Table 4 present the calculated values of bandgap narrowing (ΔE_{BGN}),

effective bandgap energy (E_{geff}), and cutoff wavelength (λ_{cut}) for the two compositions investigated at the different doping levels considered, ranging from the absence of BGN to the heavily doped regime (3×10^{18} cm^{-3}).

Table 3. Physical parameters for $x = 0.12$ ($In_{0.12}Ga_{0.88}N$), $T = 300$ K.

N [cm^{-3}]	Doping Regime	ΔE_{BGN} [meV]	E_{geff} [eV]	λ_{cut} [nm]	$\Delta\lambda$ [nm]
No BGN	—	0	2.9524	420.0	—
10^{16}	Low	5.15	2.9473	420.7	+0.7
10^{17}	Low-to-moderate	35.6	2.9168	425.2	+5.2
5×10^{17}	Moderate	150.0	2.8024	442.5	+22.5
10^{18}	High	283.7	2.6687	464.7	+44.8
3×10^{18}	Very High	792.0	2.1604	574.0	+154

Table 4. Physical parameters for $x = 0.28$ ($In_{0.28}Ga_{0.72}N$), $T = 300$ K.

N [cm^{-3}]	Doping Regime	ΔE_{BGN} [meV]	E_{geff} [eV]	λ_{cut} [nm]	$\Delta\lambda$ [nm]
No BGN	—	0	2.3692	523.4	—
10^{16}	Low	6.24	2.3630	524.8	+1.4
10^{17}	Low-to-moderate	43.30	2.3259	533.2	+9.8
5×10^{17}	Moderate	186.5	2.1827	568.1	+44.7
10^{18}	High	240.7	2.1285	582.7	+59.3
3×10^{18}	Very High	993.5	1.3757	901.4	+378

3.2. Evolution of Band Gap Narrowing with Doping

Figure 1 illustrates the evolution of ΔEBGN_{BGN}BGN as a function of the doping concentration for the two Indium mole fractions. A strongly non-linear increase in the BGN is observed: negligible at low doping levels (<5.15 meV at 10^{16} cm^{-3} for $x = 0.12$), it becomes critical beyond 10^{18} cm^{-3}, reaching 792.0 meV and 993.5 meV for $x = 0.12$ and $x = 0.28$, respectively, at 3×10^{18} cm^{-3}.

In general, the composition $x = 0.28$ exhibits a larger BGN than $x = 0.12$, particularly at low and very high doping levels. However, an exception is observed at $N = 10^{18}$ cm^{-3}, where the calculated BGN for $x = 0.12$ (283.7 meV) slightly exceeds that of $x = 0.28$ (240.7 meV). This deviation may arise from the interplay between effective mass and dielectric screening effects in the Jain–Roulston formulation.

3.3. Reduction of the Effective Bandgap Energy

Figure 2 shows the evolution of Egeff with doping. For $x = 0.12$, Egeff decreases from 2.9524 eV (without BGN) to 2.1604 eV at 3×10^{18} cm^{-3}, representing a reduction of 26.8%. For $x = 0.28$, the drop is even more pronounced: from 2.3692 eV to 1.3757 eV, corresponding to a reduction of 41.9%.

These significant reductions in Egeff can disrupt band alignment in multi-junction structures and alter the ideal diode quality factor, directly impacting the fill

factor FF and the conversion efficiency η of the solar cell [4] [8].

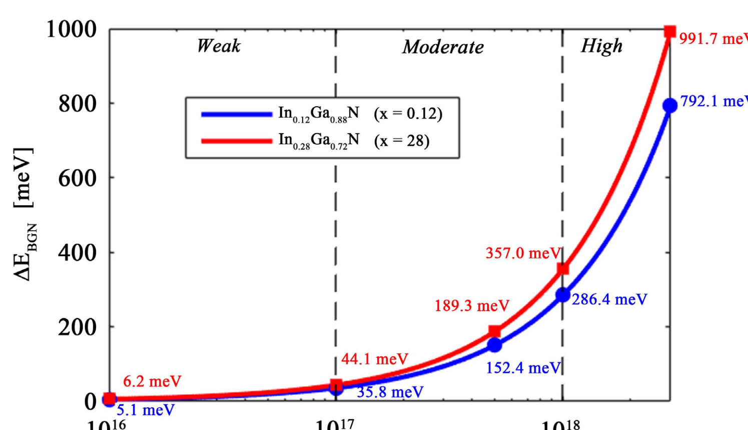

Figure 1. Variation of band gap narrowing ΔE_{BGN} as a function of doping concentration N for $x = 0.12$ and $x = 0.28$ at $T = 300$ K.

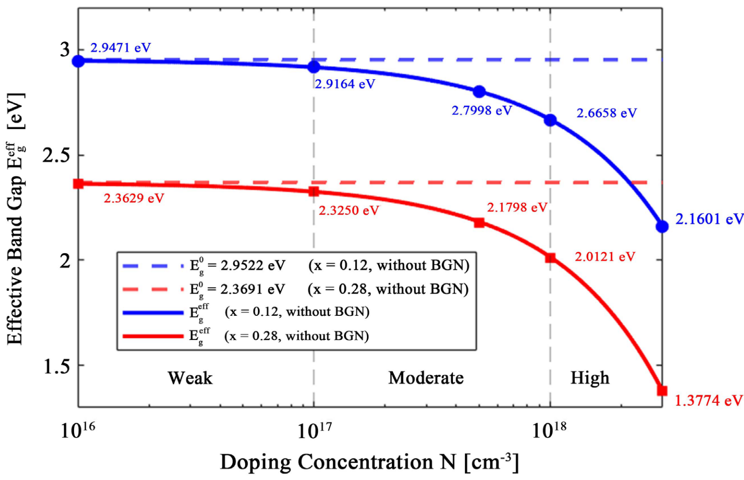

Figure 2. Effective bandgap energy E_{geff} as a function of doping concentration N for the two InGaN compositions.

3.4. Shift of the Cutoff Wavelength

Figure 3 shows the evolution of λ_{cut} with doping. The red shift is moderate at low doping levels but becomes spectacular in the high doping regime. For $x = 0.28$, λ_{cut} increases from 523.4 nm to 901.4 nm, crossing the visible-infrared boundary of the solar spectrum. This significantly broadens the spectral absorption window.

3.5. Summary of the Spectral Shift $\Delta\lambda_{cut}$

Table 5 and **Figure 4** summarize the shifts in $\Delta\lambda_{cut}$ relative to the reference case (without BGN) for each doping regime. The comparison between the two compositions shows that $x = 0.28$ consistently produces a larger shift, with an amplification factor of approximately 2 to 2.5 in the moderate and high doping regimes, reaching a factor greater than 2.4 in the very high doping regime.

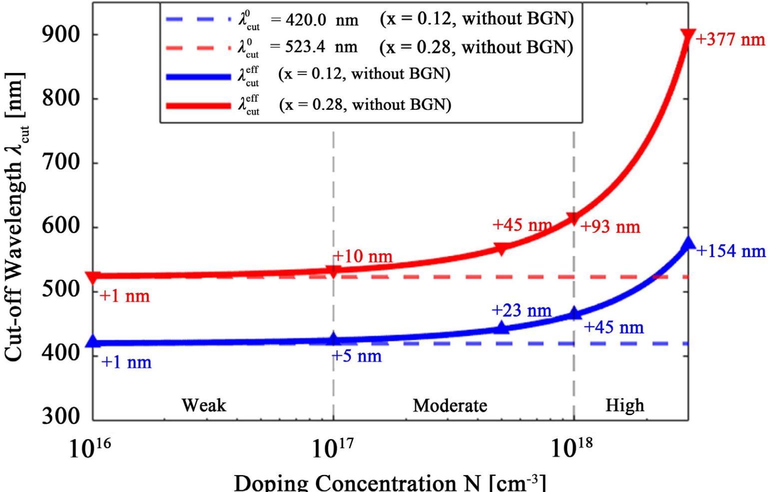

Figure 3. Cutoff wavelength λ_{cut} as a function of doping concentration N. The redshift is more pronounced for $x = 0.28$.

Table 5. Shift $\Delta\lambda_{cut}$ of the cutoff wavelength according to the doping regime.

Doping Regime	Concentration N [cm^{-3}]	$x = 0.12$: $\Delta\lambda_{cut}$ [nm]	$x = 0.28$: $\Delta\lambda_{cut}$ [nm]
Low	10^{16}	+0.7	+1.4
Moderate	5×10^{17}	+22.5	+44.7
High	10^{18}	+44.7	+59.3
Very High	3×10^{18}	+154	+378

$\Delta\lambda_{cut}$ calculated with respect to the reference case without BGN for each composition.

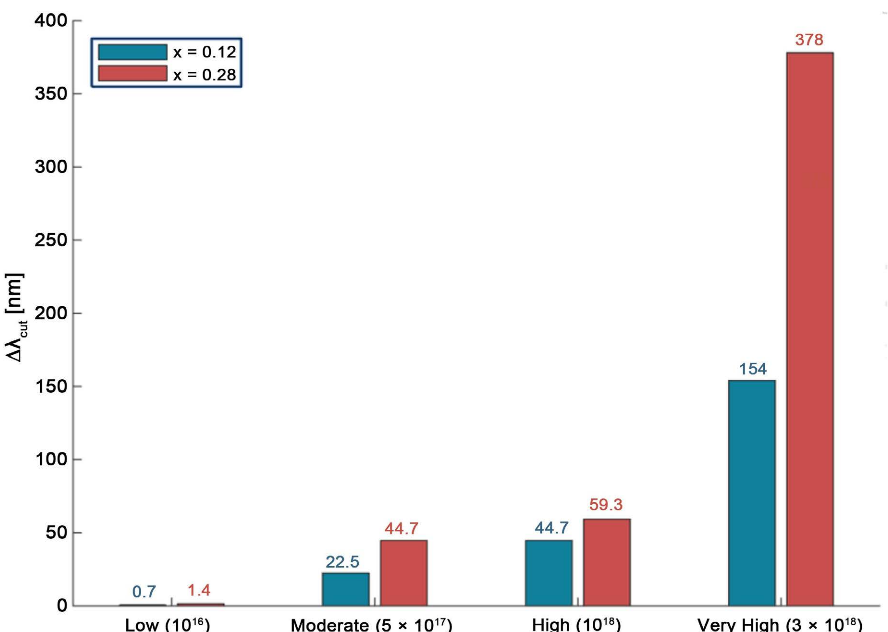

Figure 4. Spectral shift $\Delta\lambda_{cut}$ by doping regime for $x = 0.12$ and $x = 0.28$. The nonlinearity is particularly pronounced in the very heavy regime.

3.6. Implications for Photovoltaic Optimization

The analysis shows that doping in the range of 10^{16} - 5×10^{17} cm^{-3} enables a moderate spectral extension ($\Delta\lambda_{cut}$ < 45 nm for both compositions) while keeping the effective bandgap energy close to the nominal values. This regime therefore represents an optimal doping window for taking advantage of BGN without severely compromising the material's electronic properties, in line with several recent studies on InGaN cell optimization [6]-[9].

Beyond 10^{18} cm^{-3}, the non-linear increase in BGN induces an excessive reduction in Egeff, which is likely to lower the open-circuit voltage Voc and degrade the overall efficiency of the solar cell, despite the broadening of the absorption window. An optimal compromise must therefore be determined according to the incident solar spectrum and the specific cell architecture, whether single-junction, tandem, or intermediate-band devices [4] [8] [9] [13].

4. Conclusions

This study presents a systematic numerical analysis of the Band Gap Narrowing (BGN) effect in InGaN solar cells for two Indium molar fractions ($x = 0.12$ and $x = 0.28$) at $T = 300$ K. The main results can be summarized as follows:

- BGN increases in a strongly non-linear manner with doping concentration, with a critical acceleration beyond 10^{18} cm^{-3}.
- The $x = 0.28$ composition exhibits a systematically more pronounced BGN, resulting in a greater reduction of Egeff and a larger shift in λ_{cut}.
- A maximum shift of +378 nm is observed for $x = 0.28$ at 3×10^{18} cm^{-3}, moving λ_{cut} to 901.4 nm in the near-infrared region.
- The optimal doping range for photovoltaic applications lies between 10^{16} and 5×10^{17} cm^{-3}, providing a good compromise between spectral extension and material quality.

These results constitute an essential quantitative foundation for the design of high-efficiency InGaN solar cells. Future work will incorporate the effects of temperature, the internal piezoelectric electric field inherent to nitrides, and layer morphology on the effective BGN, in connection with recent advances reported for advanced InGaN structures [3] [4] [13].

Conflicts of Interest

The authors declare no conflicts of interest regarding the publication of this paper.

References

[1] Wu, J., Walukiewicz, W., Yu, K.M., Shan, W. and Ager III, J.W. (2003) Superior Radiation Resistance of $In_{1-x}Ga_xN$ Alloys. *Journal of Applied Physics*, **94**, 6477-6482. https://doi.org/10.1063/1.1618353

[2] Bhuiyan, A.G., Sugita, K., Hashimoto, A. and Yamamoto, A. (2012) InGaN Solar Cells: Present State of the Art and Important Challenges. *IEEE Journal of Photovoltaics*, **2**, 276-293. https://doi.org/10.1109/jphotov.2012.2193384

[3] Zhao, Y., Xu, M., Huang, X., Lebeau, J., Li, T., Wang, D., *et al.* (2023) Toward High Efficiency at High Temperatures: Recent Progress and Prospects on InGaN-Based Solar Cells. *Materials Today Energy*, **31**, Article 101229. https://doi.org/10.1016/j.mtener.2022.101229

[4] Marouf, Y., Dehimi, L., Bencherif, H., Pezzimenti, F., Younsi, Z., Albaqami, M.D., *et al.* (2025) Deep Insights on the Performance of Different Structures of InGaN-Based Tandem Photovoltaic Cells: Path Towards the Design of High Efficiency PV Modules. *Journal of Optics*, **54**, 3326-3341. https://doi.org/10.1007/s12596-024-02045-z

[5] Jain, S.C. and Roulston, D.J. (1991) A Simple Expression for Band Gap Narrowing in Heavily Doped Si, Ge, GaAs and Ge_xSi_{1-x} Strained Layers. *Solid-State Electronics*, **34**, 453-465. https://doi.org/10.1016/0038-1101(91)90149-s

[6] Parajuli, D., Shah, D.K., KC, D., Kumar, S., Park, M. and Pant, B. (2023) Influence of Doping Concentration and Thickness of Regions on the Performance of InGaN Single Junction-Based Solar Cells: A Simulation Approach. *Electrochem*, **3**, 407-415. https://doi.org/10.3390/electrochem3030028

[7] El Ghazi, H., Eker, Y.R., En-nadir, R., Zaki, S.E. and Basyooni-M. Kabatas, M.A. (2024) Enhancing Performance of Polar InGaN-Based Thin Film Solar Cells through Intrinsic Layer Impact Optimization: Numerical Modeling. *Results in Engineering*, **21**, Article 101909. https://doi.org/10.1016/j.rineng.2024.101909

[8] Wei, Z., Al-Nuaimi, N. and Gemming, S. (2024) Optimization of InGaN-Based Solar Cells by Numerical Simulation: Enhanced Efficiency and Performance Analysis. *Next Materials*, **6**, Article 100325. https://doi.org/10.1016/j.nxmate.2024.100325

[9] Alhejji, M., Alavijeh, M., Kupernik, J., *et al.* (2025) Investigating the Efficiency of InGaN p-n-p-n Homojunction Solar Cells. *MRS Advances*, **10**, 2113-2118. https://doi.org/10.1557/s43580-025-01419-0

[10] Vegard, L (1921) Die Konstitution der Mischkristalle und die Raumfüllung der Atome. *Zeitschrift für Physik*, **5**, 17-26. https://doi.org/10.1007/bf01349680

[11] Moses, P.G. and Van de Walle, C.G. (2010) Band Bowing and Band Alignment in InGaN Alloys. *Applied Physics Letters*, **96**, Article 021908. https://doi.org/10.1063/1.3291055

[12] Levinshtein, M., Rumyantsev, S. and Shur, M. (2001) Properties of Advanced Semiconductor Materials: GaN, AlN, InN, BN, SiC, SiGe. Wiley.

[13] Abboudi, H., En-Nadir, R. and Basyooni, M.A. (2024) Enhancing the Photovoltaic Efficiency of $In_{0.2}Ga_{0.8}N$/GaN Quantum Well Intermediate Band Solar Cells Using Combined Electric and Magnetic Fields. *Materials*, **17**, Article 5219. https://doi.org/10.3390/ma17215219